

Final Report

GR/M20402/01

High Resolution Ion Imaging Studies of Molecular Photodissociations

Background

The summary objective from the Case for Support of the original application was as follows:

This proposal seeks funding to allow a number of modifications to the existing ion imaging apparatus. These include: redesigning the main reaction chamber so that the parent molecular beam is directed at, rather than at right angles to, the detector; attaching vacuum feedthrough micrometer adjusts to the extraction electrode assembly to enable fine tuning of the image position on the microchannel plates (MCPs); reconfiguring the extraction fields so that the TOF section can be at ground potential; adding a gate valve at the end of the flight tube, just before the MCPs, so that each venting of the chamber does not necessitate laborious and time consuming reconditioning of the MCPs; and replacing the diffusion pumps on the main chamber with turbomolecular pumps to reduce unwanted background ion signal. These modifications should result in a state-of-the-art, high resolution, ion imaging apparatus which will be used to (i) study the primary photodissociation dynamics of a number of triatomic and small polyatomic molecules and (ii) start detailed explorations of the origins and mechanisms of recently observed correlations between the recoil velocity vector (\mathbf{v}) and the angular momentum vector (\mathbf{J}) of atoms produced in the photolysis of simple diatomic and triatomic systems.

The proposal sought relatively modest equipment/consumables funding, plus a contribution towards the salary of a technician and a studentship. In the event, all but the studentship was awarded. This decision was seemingly based on the fact (flagged in the proposal) that the Bristol group had recently been awarded 3 years funding for postdoctoral fellow to undertake ion imaging work within the EU TMR network IMAGINE. The fact that the two projects had different scientific objectives seemed not to matter! This left me in an awkward position, since it seemed unlikely that the one PDRA would have time to attempt to satisfy all objectives listed in both proposals. In the event we gambled, accepted EPSRC grant GR/M20402, embarked on redesigning the imaging spectrometer, and submitted a further application to EPSRC for funding for a project student to work on the resulting apparatus. Fortunately this subsequent application was successful (GR/M70186, start date 1/4/00) and, apart from our having thus far concentrated largely on diatomic (rather than small polyatomic systems), all of the above objectives have been achieved – to a higher standard than I would have dared hope at the outset. This is in large part due to the skill and determination of the EU funded PDRA's (Dr Eckart Wrede for 2 years, and Dr Eloy Wouters, in the third year), the EPSRC supported project student, Mr Marco Beckert, and various undergraduate students who have at various times assisted with the project.

1. Spectrometer design

We had more good fortune at the outset of the project – namely the demonstration, by the Nijmegen group,¹ of the improved image resolution that can result from operating the spectrometer under so called ‘velocity mapping’ conditions. We were thus able to design (using the SIMION 6 software package) and accommodate an appropriate set of annular extraction electrodes within our spectrometer re-design. The eventual spectrometer is shown in fig. 1.

The spectrometer comprises: (i) a differentially pumped source chamber from which exits a pulsed, skimmed supersonic molecular beam of the parent molecule of interest (typically a few percent seeded in Ar, at a backing pressure of ~760 Torr), (ii) a separately pumped photolysis chamber, equipped with three separately biased, annular electrodes optimised for velocity mapping, surrounded by a grounded, liquid nitrogen cooled copper cryo-shield to provide additional pumping of the source region, (iii) a TOF region, and (iv) a separately pumped detector chamber (which can be separated from the remainder of the experiment by a manually operated gate valve) housing a matched pair of 40 mm diameter active area microchannel plates (MCPs) in front of a UV enhanced fast phosphor (P47) screen which is viewed by a CCD camera equipped with a time gated image intensifier (Photonic Science). Typically base pressures at operation were $1?10^{-5}$ Torr in the source chamber, $2?10^{-8}$ Torr in the photolysis chamber, and $4?10^{-8}$ Torr in the TOF and detector regions. The molecular beam is directed at the centre of the MCPs, and is designed to pass along the centre axis of the annular ion optic assembly. The photolysis and probe laser outputs are counter-propagated along an axis passing between the repeller and first extraction electrode, orthogonal to the molecular beam axis, and focused so that their respective foci overlap (in both space and time) with the early

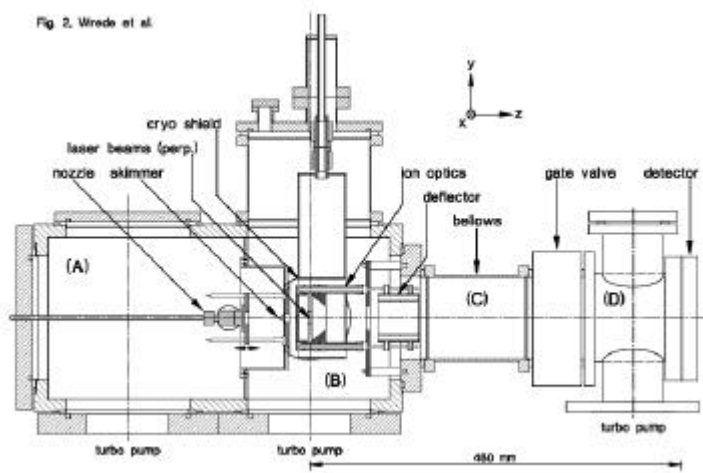


Fig. 1: Vertical cross-section through ion imaging spectrometer comprising: (A) molecular beam source chamber with pulsed nozzle; (B) photolysis chamber with ion optics and liquid nitrogen cooled cryo-shield to provide extra pumping of the source region; (C) field free TOF region; (D) detector chamber which can be separated from the remainder by a gate valve. The x,y,z axes are defined as shown (x -axis pointing into the plane). This depiction shows the spectrometer with the 'standard' flight path of $d = 460$ mm. This can be reduced to $d = 262$ mm by removing the bellows and gate valve or extended, as in the highest resolution work, to $d = 860$ mm by inserting a nipple between the detector chamber (D) and the detector flange.

time part of each expanding gas pulse. The photofragment of interest (e.g. ground state ^{79}Br and ^{81}Br atoms) are 'tagged', in the interaction region, by two photon resonance enhanced multiphoton ionisation (REMPI) and detected, isotope specifically, by monitoring just those ions impacting on the MCP/phosphor screen with the appropriate TOF. In all but the latest experiments (see below) both the photolysis and probe beams are polarised vertically in the laboratory frame, *i.e.* with their respective \hat{e} vectors parallel to the face of the detector. Each ion image resulting from a single laser shot is processed with an 'event counting' algorithm provided with the commercial camera software DaVis (LaVision – an industrial partner in the TMR network 'IMAGINE') running on a PC. This algorithm takes advantage of the finite size of an individual ion impact as it is seen by the camera (typically 2–3 pixel FWHM) by analysing 3×3 pixels around its maximum to calculate the centre of gravity for this particular event. The event is added as a single count at the appropriate (x,y) pixel co-ordinate to a buffer, and the complete image is obtained by accumulating such counts over 5000 – 10000 laser shots. The signal levels (*i.e.* events per laser shot) for each of the measurements are chosen carefully in order not to 'saturate' the event counting by multiple impacts onto the same detector position within a single laser shot and in order to minimise any blurring of the image due to space charge effects.

2. Demonstrations of the Spectrometer Resolution, and demonstrations of the breakdown of the 'axial recoil approximation'.

To investigate the ultimate resolution of the ion imaging technique, and our newly constructed spectrometer, we undertook a detailed investigation of the near threshold dissociation of jet-cooled IBr molecules. Fig. 2 shows raw images (left hand column) and 2-D slices through reconstructed 3-D recoil distributions (centre column) of ground state ^{79}Br atoms resulting from photolysis of jet-cooled I^{79}Br molecules at four different wavelengths, λ_{phot} , in the range 660–682 nm.² Two points are immediately evident. First, the raw images obtained with the new apparatus are sharp and symmetrical – thereby demonstrating that we had succeeded in our primary objective of building an ion imaging spectrometer of unprecedented energy resolution. Indeed, at the time this data was taken (late 1999), we believe that this spectrometer out-performed all others in the world in terms of image fidelity and resolution. Several other (mainly U.S.) groups have since constructed similar (and in some cases) larger spectrometers that approach ours in resolution and performance. The second point to note is that the maximum in each angular distribution is at 90° to the \hat{e} vector of the photolysis radiation, consistent with a presumed $\text{A}(1) \rightarrow \text{X}(0^+)$ perpendicular excitation in the IBr parent. Details of the observed recoil anisotropy is discussed in more detail below.

The corresponding velocity distributions are shown to the right of each image in Fig. 2. Each displays two or more clear rings in pixel (velocity) space, the respective radii of each of which decreases with increasing excitation wavelength. These rings are due to dissociation following excitation of IBr(X) molecules in their ground and first few excited vibrational levels. The innermost ring in each case arises from dissociation of $v'' = 0$ molecules. The intense neighbouring ring at higher velocity is associated with dissociation of molecules with $v'' = 1$, while careful inspection of the images taken at the longest excitation wavelengths reveals weak third and even fourth rings due to fragmentation of molecules with $v'' = 2$ and 3. The relative intensities of these peaks, and their variation with excitation wavelength, reflects the relative populations of the v'' levels in the molecular beam, convoluted by the respective Franck-Condon factors for the $\text{A}(1) \rightarrow \text{X}(0^+, v'')$ free \rightarrow bound transition at each λ_{phot} .

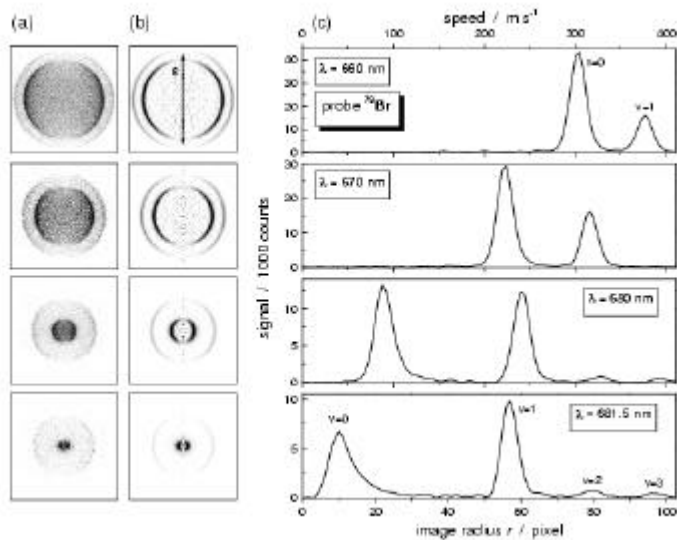


Figure 2: (a) Raw ion images and (b) 2-D slices through the reconstructed 3-D recoil distributions of ground state ^{79}Br atoms from the photolysis of jet-cooled I^{79}Br molecules. z denotes the electric vector of the photolysis light (*i.e.* axis of cylindrical symmetry).

(c) Corresponding velocity distributions.

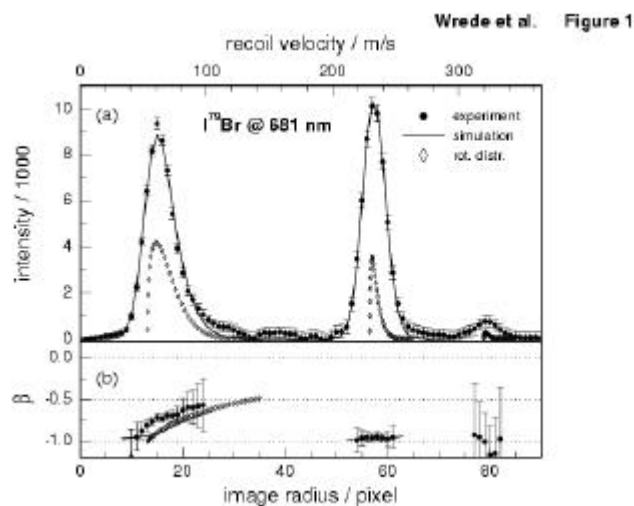


Figure 3 (a) Velocity distribution of ^{79}Br atoms from the photodissociation of IBr at 681.0 nm. Superimposed is a best-fit simulation based upon the convolution of the rotational state population distributions for parent I^{79}Br molecules with $v''=0, 1$ and 2, and $T_{\text{rot}} = 12$ K. The contribution (?) from each parent quantum state has been convoluted with a Gaussian of 4.6 pixels FWHM. (b) A comparison of the measured variation of the measured anisotropy parameter (β , corrected using the procedures outlined in the Appendix to ref. 3) with the rotational level dependence of β predicted by the quasi-classical calculations (β , shown for $v''=0$ only), and its weighted distribution (β , for $v''=0$ and 1).

As fig. 3 shows, for the specific case of the ^{79}Br atoms from the photodissociation of IBr at 681.0 nm, the measured ^{79}Br product velocity distributions are reproduced very well by simulations which involve contributions from dissociation of parent I^{79}Br molecules in all rovibrational populated in our supersonic molecular beam. The contribution from each parent quantum state is convoluted with a Gaussian of 4.6 pixels FWHM to mimic the deduced experimental resolution. Implicit in this analysis is a determination of the precise kinetic energy of the fragments resulting from photolysis of parent molecules with $v''=J''=0$. Knowing the photon energy, simple energy conservation gives a value for the bond dissociation energy $D_0(\text{I}^{79}\text{Br})$. As shown in ref. 2, the uncertainty on this value can be further reduced by simultaneous analysis of data sets taken at several near threshold excitation wavelengths, ultimately yielding a dissociation energy value of unprecedented precision: $D_0(\text{I}^{79}\text{Br}) = 14798 \pm 1 \text{ cm}^{-1}$.

The lower panel in fig. 3 shows the way in which the recoil anisotropy parameter, β , deduced by fitting the angular distribution of ^{79}Br fragments in terms of the expression $\{1 + \beta P_2(\cos \theta)\}$, where θ is the angle between the electric vector of the photolysis radiation and the direction of fragment recoil, varies with recoil velocity.⁴ The limiting value of β for a perpendicular parent excitation, such as here, is $\beta=1$. Fragments from dissociation of IBr molecules with $v''=1$ show such limiting anisotropy, but careful inspection of the image of the slow fragments resulting from dissociation of $\text{IBr}(v''=0)$ molecules show those with larger recoil velocities to have a noticeably reduced angular anisotropy. Given the monochromaticity of the photolysis radiation, increased recoil velocity of fragments resulting from photolysis of $v''=0$ molecules can only derive from increased parent internal (rotational) energy. This data (and analogous data for Br atoms resulting from near threshold dissociation of Br_2 molecules (via a parallel transition) can be understood in terms of breakdown of the axial

recoil approximation as applied to the photodissociation of a diatomic molecule. As the lower panel of fig. 3 illustrates, the data can be reproduced, quantitatively, using both quantum and semi-classical methods together with the best available potential energy curves for the relevant excited states of IBr (and Br_2).³ This study, which provides a particularly clear and direct visualisation of the breakdown of the axial recoil approximation in a near threshold dissociation process, provides further illustration of the fidelity and resolution of the new ion imaging spectrometer.

3. Continuum State Spectroscopy

IBr molecules show broad, continuous absorption throughout the visible region, and their fragmentation following excitation in this wavelength range has long been a source of fascination to both experimentalists and theoreticians, not least because of the mixed adiabatic-diabatic picture required in order to interpret its spectroscopy and predissociation dynamics.^{5,6} Many details regarding the number and symmetry of the excited states contributing to the excitation and fragmentation process remained unclear, however. To provide further illustration of the power of high resolution ion imaging spectroscopy to ‘look within’ apparently featureless absorption continua we thus carried out a comprehensive study of the photolysis of jet-cooled IBr molecules at numerous excitation wavelengths in the range 440–685 nm.⁷ Image analysis provided precise values for the electronic branching into ground [$\text{I}(^2\text{P}_{3/2})+\text{Br}(^2\text{P}_{3/2})$] and excited [$\text{I}(^2\text{P}_{3/2})+\text{Br}(^2\text{P}_{1/2})$] products, and the recoil anisotropy of each set of products, as a function of excitation wavelength. As fig. 4 illustrates, such experimental data enabled us to map out the wavelength dependent partial cross-sections for parallel ($\theta = 0$) and perpendicular ($\theta = 90^\circ$) absorptions, and thus deconvolute the parent absorption spectrum into contributions associated with excitation to the $\text{A}^3\Pi(1)$, $\text{B}^3\Pi(0^+)$ and $\text{C}^1\Pi(1)$ excited states of IBr. Such analyses of the continuous parent absorption spectrum, taken together with previous spectroscopic data for the bound levels supported by the A and B state potentials, allowed determination of the potential energy curves for, and (R independent) transition moments to, each of these three excited states – which served to highlight the rather severe limitations of previous theoretical estimates of the form of these potentials. Wavepacket calculations

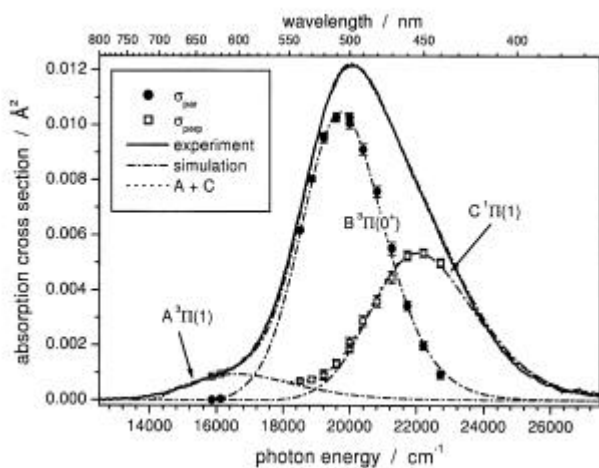


Figure 4 Optimum deconvolution of the total room temperature absorption spectrum of IBr (bold curve) into $\sigma_{\text{A-X}}(\theta)$, $\sigma_{\text{B-X}}(\theta)$ and $\sigma_{\text{C-X}}(\theta)$ partial cross-sections using the potentials shown in fig. 5 and parameterised in Table I of ref. 7. The symbols θ and θ show, respectively, the experimentally derived cross-sections for parallel, σ_{par} , and perpendicular absorption, σ_{perp} . The ‘steps’ in the $\sigma_{\text{A-X}}$ curve at $\sim 14500 \text{ cm}^{-1}$ correspond to the dissociation limits for $\text{IBr}(v'' = 0, 1, \dots) \rightarrow \text{I} + \text{Br}$ and are an artefact of the output of the wavepacket calculation.

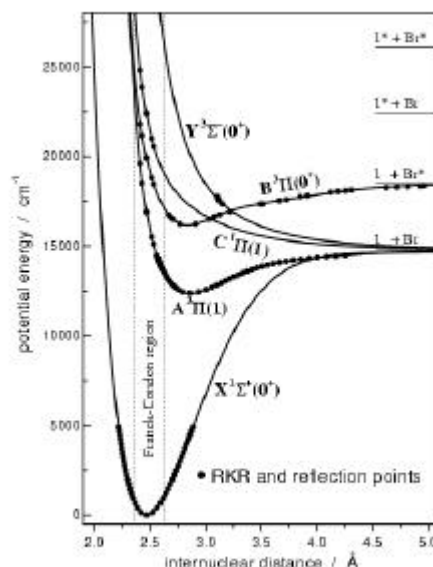


Fig. 11, Wade et al.

Figure 5 Diabatic potential energy curves for the X, A, B and C states of IBr derived in the present work. Also shown, for completeness, is the assumed location of the diabatic Y state potential responsible for the predissociation of the higher v' levels of the B state. The RKR points were taken from a variety of sources as detailed in ref. 7

employing these excited state potential energy functions reproduced, quantitatively, the experimentally determined wavelength dependence of these product branching ratios and product recoil anisotropies, thereby confirming the accuracy of the derived potentials and defining the value (120 cm^{-1}) of the coupling matrix element coupling the bound (B) and dissociative (Y) diabatic states of σ symmetry. A similarly extensive ‘continuum state spectroscopy’ study of the related interhalogen BrCl – in which spin-orbit effects are much smaller, and the analogous $B \rightarrow Y$ coupling occurs at much larger R – is now largely complete.

4. Quantification of product orientation, alignment and the determination of ‘alignment-free’ recoil anisotropies in molecular photodissociations.

It is now appreciated that fragments arising in molecular dissociations may be aligned (*i.e.* product states with different M_J may be unequally populated) or, in appropriate circumstances, oriented (states with $+M_J$ and $-M_J$ quantum numbers are unequally populated). Such inequalities can arise as a result of interference effects in the excited state preparation, or as a result of non-adiabatic couplings as the excited molecules evolve towards the asymptotic products. Measurement and interpretation of such fragment orientation and alignment effects (which can also be viewed in terms of correlations between the velocity \mathbf{v} and angular momentum \mathbf{J} vectors of the products) can provide another stringent test of both the molecular potentials and, even more revealingly, the non-Born-Oppenheimer couplings between them, and constitutes something of a ‘hot topic’ in this area of contemporary chemical physics. Two related experimental issues needed to be confronted. Firstly, there is a need for experimentally convenient and robust protocols to enable study and quantification of such correlations. Second, even if such subtleties are not the main focus of a photolysis study, it remains the case that *if* (as will often be the case) the nascent fragments arising in a molecular dissociation are oriented or aligned, then the choice of probe transition, probe laser polarisation and experimental geometry may well influence the detected signal, whether the user intends it or not. Once again, therefore, quantifying and understanding the role of the \mathbf{v} , \mathbf{J} correlation will be necessary simply to establish more basic quantities like recoil anisotropy and product branching ratios.

Ion imaging methods are particularly suited to revealing \mathbf{v} , \mathbf{J} correlation and, consistent with the original proposal, the measurement and quantification of these effects has been a major recent objective. BrCl was chosen as a convenient test molecule, since both atomic fragments have $J = 3/2$ ground states and are thus capable of exhibiting both orientation and alignment effects. Photolysis of jet-cooled BrCl molecules was investigated at four different wavelengths in the range 425–485 nm by high resolution velocity map ion imaging.⁸ At each wavelength, four images of the $\text{Cl}(^2P_{3/2})$ atomic fragments were recorded using counterpropagating photolysis and probe laser beams, with θ_{phot} aligned perpendicular to the detection axis and the probe laser polarization, respectively, linearly aligned and vertical (*i.e.* parallel to θ_{phot} and perpendicular to the detection axis), right circularly polarized, horizontally linearly polarized (*i.e.* parallel to the detection axis) and left circularly polarized on successive laser shots. These different probe laser polarisations were achieved using a home built pulsed high voltage supply and a modified Pockel’s cell. Recording the four images in this way – another experimental first to the best of our knowledge – ensures that they are automatically self-normalised with respect to any medium term drift in the experimental conditions. Appropriate linear combinations of the images allow quantification of the alignment of the $\text{Cl}(^2P_{3/2})$ fragments in terms of the alignment anisotropy parameters s_2 , β_2 , β_2 and β_2 advanced by Vasyutinskii and coworkers,⁹ as a function of parent excitation wavelength; another combination provides a convenient route to the true ‘alignment-free’ recoil anisotropy parameter, β_0 . Fig. 6 provides illustrative measured and combination images, for the case of BrCl photolysis at 467.16 nm. The parameter values so derived have been interpreted⁸ in terms of both incoherent and coherent contributions to the alignment, with both simultaneous parallel and perpendicular excitations to the $B^3\sigma(0^+)$ and $C^1\sigma(1)$ states and excitations to the $\beta = \beta_1$ components of the C state contributing to the latter. The deduced values of the alignment-free β parameters indicate (wavelength dependent) contributions from both parallel and perpendicular parent absorptions in this wavelength range. Such a conclusion accords with our latest deconvolutions of the parent absorption spectrum, and with our very recent determination of the orientation parameter β_1 obtained by fitting the difference image obtained in another proving experiment (involving BrCl photodissociation at 480.63 nm) when using left and right circularly polarised radiation to probe the $\text{Cl}(^2P_{3/2})$ atoms and θ_{phot} aligned at 45° to the detection axis.

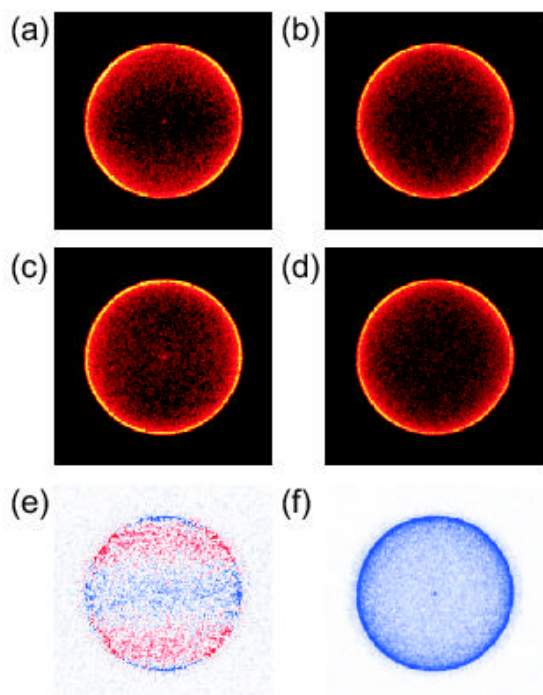


Figure 6 Raw images of $\text{Cl}(^2\text{P}_{3/2})$ atoms from photolysis of jet-cooled BrCl molecules at 467.16 nm with $\theta_{\text{phot}} // \text{Y}$ (*i.e.* perpendicular to the TOF axis). The probe laser radiation, which propagates along X is polarised (a) linearly along Y, (b) right circularly (R), (c) linearly along Z (the TOF axis) and (d) left circularly (L). The colour map of images (b) and (d) has been downscaled by a factor of 1.5 to account for the fact that the images obtained with circularly polarized probe light contain $\sim 1.5\times$ as much signal. (e) and (f) show the alignment difference image $\{M_Z - M_Y\}$ (plotted using the convention blue = +ve, white = 0 and red = -ve) and the alignment-free combination image $\{M_Y + M_Z\} \frac{1}{3}(M_L^X + M_R^X)$.

Research Impact, Explanation of Expenditure and Further Research and Dissemination Activities

The high resolution ion imaging work has been described in several presentations at international conferences (*e.g.* XXIV Informal Photochemistry Conference, Puerto Rico, 4/00; Gordon Conference on 'Atomic and Molecular Interactions', New Hampshire, U.S.A.; 7/00, Chemical Society of Thailand Annual Conference, Bangkok, 12/00; Optical Society of America Annual Meeting/ILS-XVII, Long Beach, California, 10/01), and at various smaller national meetings, while the alignment and orientation studies will be presented at the 223rd ACS National Meeting, Orlando, Florida (4/02) and at another Gordon Conference this summer (7/02). As described more fully in the scientific report (above), this programme of work has defined new standards both in terms of image resolution and fidelity and, more recently, in the quantitative determination of alignment and orientation images. This level of achievement would not have been possible without the financial support of both EPSRC *and* the EU TMR programme, nor would the work have been anything like so complete without the substantial input offered by other members of the Molecular Science Group at Bristol (notably Dr A.J. Orr-Ewing and Profs. G.G. Balint-Kurti and R.N. Dixon). Expenditure was as originally planned. Research in this area will continue courtesy of EPSRC grant GR/M70186 and additional EU funding through the TMR network PICNIC coordinated by Dr. B.J. Whitaker (Leeds).

References

- ¹ A.T.J.B. Eppink and D.H. Parker, *Rev. Sci. Instrum.* **68** (1997) 3477
- ² E. Wrede, S. Laubach, S. Schulenburg, A.J. Orr-Ewing and M.N.R. Ashfold, *Chem. Phys. Lett.* **326**, 22 (2000).
- ³ E. Wrede, E.R. Wouters, M. Beckert, R.N. Dixon and M.N.R. Ashfold, *J. Chem. Phys.* **116**, xxxx (2002).
- ⁴ R.N. Zare, *Angular Momentum. Understanding Spatial Aspects in Physics and Chemistry* (Wiley, New York, 1988) and references therein.
- ⁵ M.S. Child and R.B. Bernstein, *J. Chem. Phys.* **59**, 5916 (1973).
- ⁶ M. Shapiro, M.J.J. Vrakking and A. Stolow, *J. Chem. Phys.* **110**, 2465 (1999) and references therein.
- ⁷ E. Wrede, S. Laubach, S. Schulenburg, A. Brown, E.R. Wouters, A.J. Orr-Ewing and M.N.R. Ashfold, *J. Chem. Phys.* **114**, 2629 (2001) and references therein.
- ⁸ E.R. Wouters, M. Beckert, L.J. Russell, K.N. Rosser, A.J. Orr-Ewing, M.N.R. Ashfold and O.S. Vasyutinskii, *J. Chem. Phys.* (submitted).
- ⁹ E.R. Wouters, M. Ahmed, D.S. Peterka, A.S. Bracker, A.G. Suits and O.S. Vasyutinskii, in *Imaging in Chemical Dynamics* (A.G. Suits and R.E. Continetti, eds.), *ACS Symp. Ser.* **770**, 238 (2001) and references therein.